Electron doping effects in conducting Sr_2FeMoO_6

Y. Moritomo
CIRSE, Nagoya University, Nagoya 464-8601, Japan

Sh. Xu, T. Akimoto, and A. Machida
Department of Crystalline Materials Science, Nagoya University, Nagoya 464-8603, Japan

N. Hamada
Faculty of Science and Technology, Science University of Tokyo, Chiba 278-8510, Japan

K. Ohoyama
Institute for Materials Research, Tohoku University, Sendai 980-8577, Japan

E. Nishibori, M. Takata, and M. Sakata
Department of Applied Physics, Nagoya University, Nagoya 464-8603, Japan
(Received 23 June 2000)

Effects of the electron doping on the magnetic and electronic properties have been investigated in the conducting double perovskite Sr_2FeMoO_6. Judging from the enhanced moment μ_{Mo} at the Mo site, the doped electrons are considered to occupy mainly the down-spin Mo4d band. Filling dependence of the saturation magnetization M_s, the spin-wave stiffness coefficient D_s and the γ coefficient are discussed on the basis of a LDA+U band calculation. We further discuss possible origins for the magnetism.

I. INTRODUCTION

The carrier doping by chemical substitution is a powerful tool for investigation of strongly correlated electron systems, especially the perovskitelike 3d and 4d transition-metal oxides. Most of the 3d transition-metal oxides with integer filling, e.g., $LaMnO_3$ and $LaCoO_3$, are insulating due to the strong on-site Coulomb repulsion U. With substitution of the divalent Sr^{2+} ions for the trivalent La^{3+} ion, however, these compounds become ferromagnetic metal due to the double exchange mechanism.[1] Even in the 4d-electron systems with reduced U value, notable physical properties have been reported.

Recently, ordered double-perovskite molybdenum oxides[2–6] A_2MMoO_6 (A is a rare-earth metal and M is a 3d transition metal) begin to attract current interest of material scientists in the applicational point of view. Actually, Kobayashi *et al.*[7] and Kim *et al.*[8] reported room-temperature magnetoresistance in Sr_2FeMoO_6 due to the intergrain tunneling.[9] Among the double-perovskite molybdenum oxides, Sr_2FeMoO_6 is most extensively studied, because high quality single crystals can be obtained by the floating-zone method.[10–12] Sr_2FeMoO_6 is ferrimagnetic and metallic with critical temperature $T_c \approx 400$ K. On the basis of a local-density approximation (LDA) band calculation,[7] the conduction band is dominated by the Mo4d level, while Fe3d-electrons behave as local spins. The investigation on the double-perovskite molybdenum oxides, however, is only at the starting point. We should clarify the interrelation between the local spins and the conductive 4d electrons to understand the physics (and to optimize the functionality) of the system.

In this paper, we have investigated the electron doping effects on the magnetic and electronic properties in the conducting double perovskite $(Sr_{2-x}La_x)FeMoO_6$. By means of the neutron powder-diffraction measurements, we have determined the respective magnetic moments, i.e., μ_{Fe} and μ_{Mo}, of $(Sr_{2-x}La_x)FeMoO_6$. The enhancement of the μ_{Mo} value with doping indicates that the doped electrons occupy mainly the Mo4$d_\downarrow$ band. With increase of the doping level x, the saturated magnetization M_s, and spin-wave stiffness coefficient D_s decrease, while the γ coefficient (electron contribution in the specific heat) increases. We observed a serious discrepancy between the rigid band model and the experimental results at larger-x region, even though this picture qualitatively reproduces the overall x dependence of M_s, α, and γ. The discrepancy is ascribed to the mixing of the Fe3$d_\downarrow$ state into the conduction band. On the basis of the above arguments, we will discuss possible origins for the magnetism of the conducting double-perovskite molybdenum oxides.

II. EXPERIMENT

A. Crystal growth

A series of crystals, $(Sr_{2-x}La_x)FeMoO_6$, were melt grown by the floating-zone furnace.[11] A stoichiometric mixture of commercial $SrCO_3$, La_2O_3, Fe_2O_3, Mo, and MoO_3 was well ground, and pressed into a rod with a size of 5 mm$\phi \times$100 mm and sintered at 1200 °C for 2 h in a flow of Ar gas. The crystal is grown at a feeding speed of $\sim$20 mm in an Ar atmosphere. Black and shiny crystals, typically 4–5 mm in diameter and $\sim$20 mm in length, were obtained. The neutron-diffraction experiment has revealed that thus obtained crystals are single domain. The actual chemical composition of the melt grown

TABLE I. Lattice constants and relative length of the Fe-O bond ($d_{Fe\text{-}O}/d_{Fe\text{-}Fe}$) of $(Sr_{2-x}La_x)FeMoO_6$ at 300 K. The crystal symmetry is tetragonal ($I4/mmm$; $Z=2$).

x	a (Å)	$d_{Fe\text{-}O}/d_{Fe\text{-}Fe}$	c (Å)	$d_{Fe\text{-}O}/d_{Fe\text{-}Fe}$	R_{wp} (%)	R_I (%)
0.00	5.5711(2)	0.244(1)	7.8996(4)	0.238(3)	2.77	7.89
0.10	5.5714(1)	0.246(2)	7.9087(3)	0.244(4)	2.63	7.05
0.20	5.5729(1)	0.243(3)	7.9071(2)	0.245(5)	3.09	5.85
0.30	5.5751(2)	0.241(3)	7.9078(3)	0.241(6)	3.50	4.45

$(Sr_{1.7}La_{0.3})FeMoO_6$ crystal was determined by the inductively coupled plasma (ICP) method, and is almost the same as the ideal values; Sr:La:Fe:Mo=1.692 (1.7: prepared value):0.316 (0.3):1.024 (1.0):0.972 (1.0).

B. Sample characterization

In order to characterize thus obtained crystals, synchrotron radiation x-ray powder experiments were carried out at SPring-8 BL02B2 to obtain the powder patterns with good counting statistics and high angular resolution. The inner region of the crystal ingot was crushed into a fine powder and were sealed in a 0.2 mmϕ quartz capillary. Precipitation method was adopted[13] in order to get a fine powder, which gives a homogeneous intensity distribution in a Debye-Scherrer powder ring. The wavelength of the incident x ray was ≈ 0.5 Å, and exposure time was for 5–10 min.

The crystal symmetry at room temperature ($\leqslant T_c$) is tetragonal ($I4/mmm$; $Z=2$). We have analyzed thus obtained x-ray patterns with RIETAN-97β program,[14] and listed the lattice parameters in Table I. We found no impurity peaks in the x-ray patterns. The final refinements are satisfactory, in which R_{wp} and R_I (reliable factor based on the integrated intensity) are fairly reduced ($R_{wp}=2.7$–3.5%, $R_I=4.5$–7.9%). We further have estimated the mixing ratio s of the B site with putting a virtual atom $(1-s)Fe^{3+}+sMo^{5+}$ $[sFe^{3+}+(1-s)Mo^{5+}]$ at [0,0,0] ([0,0,1/2]). The s value is nearly independent of x except for $x=0.3$: $s=16(1)\%$ at $x=0.0$,15(1)% at 0.1, 14(1)% at 0.2, and 21(2)% at 0.3.

C. Resistivity

For four-probe resistivity measurements, the sample was cut into a rectangular shape, typically of $2\times1\times1$ mm^3, and electrical contacts were made with a heat-treatment-type silver paint. Heat treatment has been done in a flow of Ar. Figure 1 shows temperature variation of resistivity ρ of $(Sr_{2-x}La_x)FeMoO_6$. Overall feature of the ρ-T^2 curve of the doped crystals is essentially the same as that of the parent Sr_2FeMoO_6 (thick curve). The resistivity well scales T^2 in the temperature range from ~ 50 to ~ 350 K. Such a T^2 law has been ascribed to the electron-electron scattering or the one-magnon scattering.[11,15]

III. RESULTS AND DISCUSSION

A. Doping effects on the magnetic structure

Figure 2 shows the magnetization curve of $(Sr_{2-x}La_x)FeMoO_6$ measured at 10 K. The M value of Sr_2FeMoO_6 rapidly increases with an external field, and then saturates at $M_s \approx 3.3\mu_B$ per an Fe site. The magnitude of M_s systematically decreases with increase of x, and becomes $\approx 2.4\mu_B$ at $x=0.3$. Here, we should be careful on the effects of the B-site disorder, which suppresses the absolute magnitude of M_s.[10] Since the mixing ratio s is nearly x independent, however, the doping-induced suppression of the net magnetization is intrinsic. To determine the critical temperature T_c for the magnetic transition, we further have measured temperature variation of the ac susceptibility.[16] In the inset of Fig. 3, we plotted T_c against x. T_c is nearly independent of x, and is ≈ 400 K.

In order to determine the magnetic moments for the respective sites, i.e., μ_{Fe} and μ_{Mo}, we have measured neutron powder-diffraction patterns of Sr_2FeMoO_6 and $(Sr_{1.7}La_{0.3})FeMoO_6$ with the Kinken powder diffractometer for high efficiency and high-resolution measurements, HERMES, installed at the JRR-3M reactor in Japan Atomic Energy Research Institute, Tokai, Japan.[17] Neutrons with wavelength 1.819 Å were obtained by the (331) reflection of Ge monochromater, and 12′-B-Sample-18′ collimation. Melt-grown crystal ingots (~ 5 g) were crushed into a fine powder and were sealed in a vanadium capsule with helium gas, and mounted at the cold head of the closed-cycle He-gas refrigerator.

Figure 3 shows neutron powder patterns of (a) Sr_2FeMoO_6 and (b) $(Sr_{1.7}La_{0.3})FeMoO_6$ at 15 K ($\leqslant T_c$). Magnitudes of the respective moments are determined by the

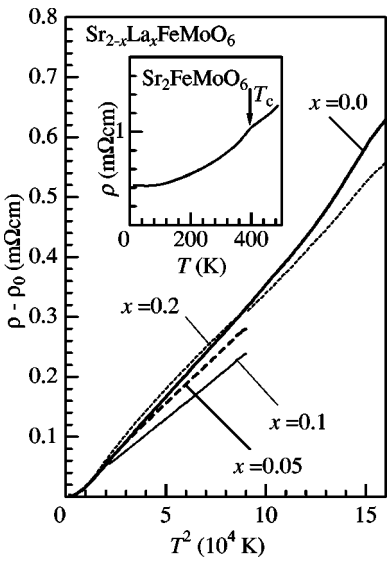

FIG. 1. Temperature variation of resistivity ρ of $(Sr_{2-x}La_x)FeMoO_6$. Note that residual resistivity ρ_0 was subtracted. Inset shows the ρ-T curve of Sr_2FeMoO_6. T_c is the critical temperature for the magnetic transition.

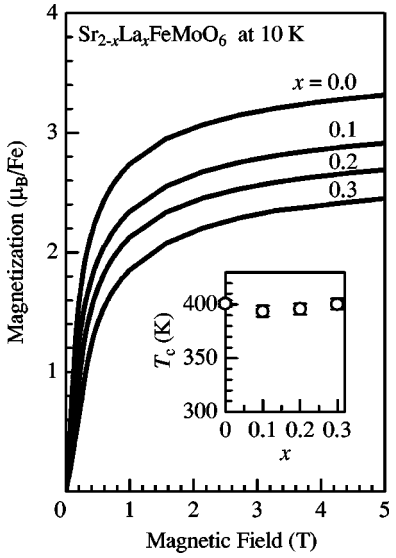

FIG. 2. Magnetization curve at 10 K of $(Sr_{2-x}La_x)FeMoO_6$. The inset shows doping dependence of the critical temperature T_c for the magnetic transition.

Rietveld fitting (RIETAN-97β, Ref. 14), in which we assume a collinear magnetic structure with spin direction along c.[18] Several impurity peaks, which are inevitably introduced from the skin region of the crystal ingot, were observed and were removed from the pattern. The obtained moments are $\mu_{Fe}=4.2(2)\mu_B$ and $\mu_{Mo}=-0.5(2)\mu_B$ at $x=0.0$, and $\mu_{Fe}=3.8(2)\mu_B$ and $\mu_{Mo}=-0.8(2)\mu_B$ at $x=0.3$. At $x=0.0$, both the moments are suppressed as compared with the ideal values ($5.0\mu_B$ and $-1.0\mu_B$ for the Fe^{3+} and Mo^{5+} ions, respectively). This is partly due to the disorder of the B-site ions. With increase of x, absolute magnitude of μ_{Mo} increases from $-0.5(2)\mu_B$ at $x=0.0$ to $-0.8(2)\mu_B$ at $x=0.3$. This enhancement of μ_{Mo} indicates that the doped electrons occupy mainly the Mo4$d_\downarrow$ band, consistently with the LDA band calculation[7] as well as the LDA+U calculation (*vide infra*).

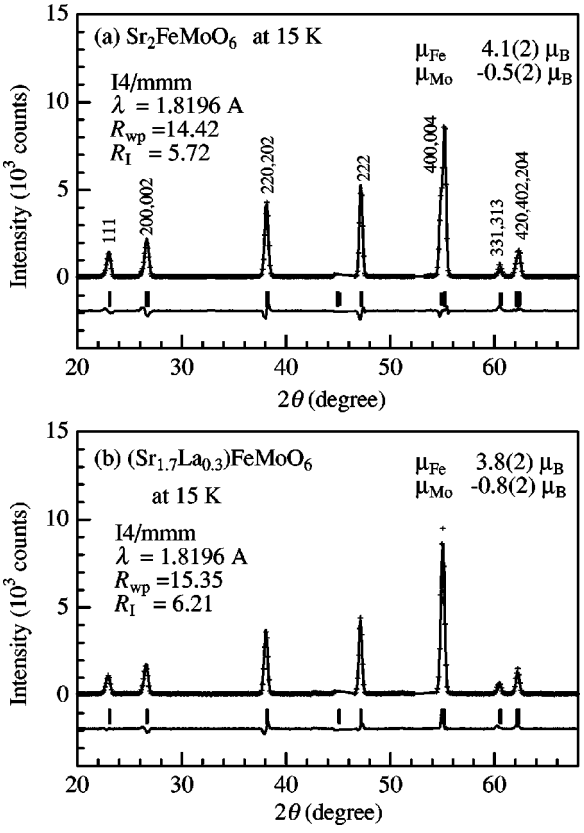

FIG. 3. Neutron powder profile of (a) Sr_2FeMoO_6 and (b) $(Sr_{1.7}La_{0.3})_2FeMoO_6$ at 15 K. Crystal structures of both the compounds are tetragonal ($I4/mmm$; $Z=2$). Solid curve is the results of the Rietveld refinement.

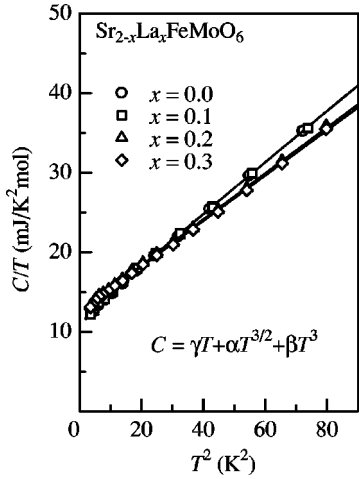

FIG. 4. Temperature dependence of the low-temperature specific heat C of $(Sr_{2-x}La_x)FeMoO_6$. Solid curves are the best fitted results taking into account of contributions from electrons, spin-waves and phonons: $C=\gamma T+\alpha T^{3/2}+\beta T^3$.

B. Doping dependence of physical properties

The electron doping has significant effects on the low-temperature specific heat C. The temperature variation of C was measured by the relaxation method, and plotted in Fig. 4 against T^2. In the magnetic compound, the total specific heat is composed of three parts, namely, contribution from the conduction electrons, the spin waves, and the phonons:

$$C=\gamma T+\alpha T^{3/2}+\beta T^3. \quad (1)$$

The solid curves in Fig. 4 are the best-fitted results. Thus obtained parameters, that is, α and γ, are plotted in Fig. 5

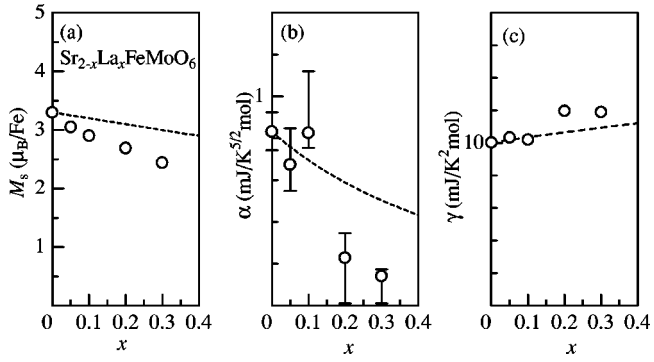

FIG. 5. Filling dependence of (a) saturation magnetization M_s, (b) α (spin-wave), and (c) γ (electron) coefficients in the low-temperature specific heat of $(Sr_{2-x}La_x)FeMoO_6$. Broken curves are results of a model calculation (see text).

against x. The parameters of Sr_2FeMoO_6 are nearly consistent with the values reported by Tomioka *et al.*[10] The thermal effective mass $m_{\rm eff}$ [$\equiv \gamma/\gamma_{\rm free}$; where $\gamma_{\rm free}$ ($=5.9$ mJ/K^2 mol) is for the free electrons per Mo site] is estimated to be ≈ 1.7. Such an enhancement of $m_{\rm eff}$ is perhaps ascribed to the electron-correlation effect. Incidentally, the magnitude of β ($\propto \Theta^{-3}$; where Θ is the Debye temperature) slightly decreases from ≈ 0.56 mJ/K^4 mol at $x=0.0$ to ≈ 0.53 mJ/K^4 mol at $x=0.3$.

The contribution of the spin waves is expressed as

$$\alpha = 0.113 k_{\rm B}(k_{\rm B}/D_{\rm s})^{3/2}, \tag{2}$$

where $k_{\rm B}$ and $D_{\rm s}$ are the Boltzmann constant and the effective spin stiffness coefficient for the acoustic branch, respectively. With use of $\alpha(=0.8$ meV Å$^{5/2})$ at $x=0.0$, $D_{\rm s}$ is estimated to be ≈ 140 meV Å^2. Taking into account of the ferrimagnetic structure, $D_{\rm s}$ is further expressed as

$$D_{\rm s} = 4|J|a^2 S_{\rm Fe} S_{\rm Mo}/(S_{\rm Fe} - S_{\rm Mo}), \tag{3}$$

where J and S_i are the exchange coupling between the Fe and Mo spins, and the spin quantum number ($=\mu_i/2$) at the i site, respectively. a ($=3.95$ Å) is the averaged lattice constant.

Here, let us argue the electron doping effects on the magnetic and electronic properties, i.e., $M_{\rm s}$, α, and γ, in terms of the rigid Mo4$d_\downarrow$ band. We summarized in Fig. 5 x dependence of (a) $M_{\rm s}$, (b) α, and (c) γ. The broken curve in Fig. 5(a) is the calculated magnetization, with assuming the decreasing $\mu_{\rm Mo}$ [$=-(1.0+x)\mu_{\rm B}$] and the constant $\mu_{\rm Fe}$ ($=+4.3\mu_{\rm B}$). We further have calculated the α value using Eqs. (2) and (3). Magnitude of $J(=-6.4$ meV) is so determined that the $D_{\rm s}$ value at $x=0.0$ becomes 140 meV Å^2. On the other hand, increase of the γ coefficient is qualitatively reproduced by the free-electron picture, i.e., $\gamma \propto n^{1/3} = (1+x)^{1/3}$ [see a broken curve in Fig. 5(c)]. Thus the rigid-band picture qualitatively reproduces the overall x-dependent feature of $M_{\rm s}$, α, and γ. We, however, observe a serious deviation of the experimental data from the calculation at larger-x region.

C. Comparison with the band calculation

Now, let us examine the electronic structure of parent Sr_2FeMoO_6. We show in Fig. 6 the density of state (DOS) for the up- and down-spin state of Sr_2FeMoO_6. We have calculated the electronic structure with the full-potential linearized augmented plane-wave (FLAPW) method[19] within the LDA+U scheme[20,21] with the effective U parameters of 2.0 eV for Fe and 1.0 eV for Mo. The actual tetragonal lattice parameters at 300 K were used (see Table I). The plane-wave cutoff energies are 12 Ry for the wave function, and 48 Ry for the potential and the charge density. We have performed the self-consistent calculation with 39 k points in the irreducible Brillouin zone for the tetragonal lattice, which correspond to 19 k points for the fcc lattice. The calculated $M_{\rm s}(=3.99\mu_{\rm B})$ and $\gamma(\approx 4.9$ mJ/mol K$^2)$ are nearly consistent with the experimental results ($M_{\rm s}=3.3\mu_{\rm B}$ and $\gamma = 10.0$ mJ/mol K^2). The generic feature is consistent with the calculation done by Kobayashi *et al.*,[7] who assumed the fcc lattice ($d_{\rm Fe-O}/d_{\rm Fe-Fe} \equiv 1/4$). One may notice very small

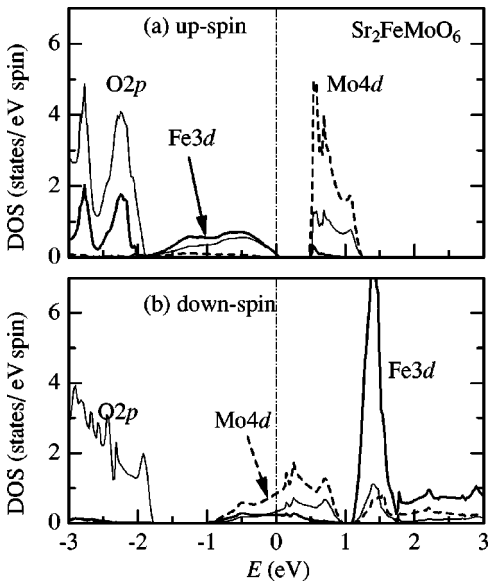

FIG. 6. Density of state (DOS) of Sr_2FeMoO_6. The electronic structure was calculated with the full-potential linearized augmented plane-wave (FLAPW) method within the LDA+U scheme with the effective U parameter of 2.0 eV for Fe and 1.0 eV for Mo. Actual tetragonal lattice parameters at 300 K were used.

but finite DOS at $E_{\rm F}$ even for the up-spin state. The partial DOS of the Fe3d state is significantly affected by the oxygen position between the Mo and Fe ions, because the shorter Fe-O bond enhances the Fe3$d(t_{2g})$-O2p hybridization.

As seen in Fig. 6(b), the down-spin conduction band near $E_{\rm F}$ is dominated by the Mo4$d_\downarrow(t_{2g\downarrow})$ state, but has a considerable amount of the Fe3$d_\downarrow(t_{2g\downarrow})$ components. This is because the Mo4$d_\downarrow(t_{2g\downarrow})$, Fe3$d_\downarrow(t_{2g\downarrow})$, and O2$p_\downarrow$ states can be hybridized via the π bonding, and can gain the kinetic energy with forming a wide conduction band. [Contrary to the down-spin band, mixing of the Mo4$d_\uparrow(t_{2g\uparrow})$ and Fe3$d_\uparrow(e_{g\uparrow})$ states is prohibited due to the different symmetry.] The mixing of the Fe3$d_\downarrow$ state can explain the deviation of the experimental data from the simple model shown in Fig. 5. In addition, the mixing is consistent with the suppressed $\mu_{\rm Fe}$ and $\mu_{\rm Mo}$.

D. Possible origins for the magnetic transition

Finally, let us discuss possible origins for the magnetism of Sr_2FeMoO_6. Historically, the ferrimagnetism of this system has been understood in terms of antiferromagnetic superexchange interaction between the $Mo^{5+}(d^1)$ spin and $Fe^{3+}(d^5)$ spins.[3–5] However, Moritomo *et al.*[6] have indicated a strong interrelation between the conductivity $\sigma_{300\rm K}$ at room temperature and $T_{\rm c}$ in Sr_2MMoO_6 (M=Cr, Mn, Fe, and Co). This implies that the conduction electrons mediate the exchange interaction between the local Fe^{3+} spins. In addition, the picture of the local Mo^{5+} spins contradicts the reduced $\mu_{\rm Mo}$ value of Sr_2FeMoO_6 [see Fig. 3(a)].

As discussed in the previous subsection, the conduction electrons have a considerable amount of the Fe3$d_\downarrow$ component. Then, the carriers can mediate the exchange interaction between the local $Fe^{3+}(d^5)$ spins via the double exchange mechanism.[1] Consistently, a characteristic cusp structure is observed at $\approx T_{\rm c}$ in the ρ-T curve of Sr_2FeMoO_6 (see the

inset of Fig. 1), indicating interrelation between resistivity and magnetic ordering. The same mechanism is applicable for Sr_2FeReO_6 ($T_c \geqslant 400$ K), whose band structure[7] is similar to that of Sr_2FeMoO_6. Note that the exchange coupling between the local $Fe^{3+}(d^5)$ spins and the carriers is *antiferromagnetic*. Then, the strong hybridization between the Mo4$d_\downarrow(t_{2g\downarrow})$ and Fe3$d_\downarrow(t_{2g\downarrow})$ states causes negative spin polarization of the Mo4d electrons.

Quite recently, Kanamori and Terakura[22] has proposed an alternative model for the magnetism of Sr_2FeMoO_6. If the Fe^{3+} spins are ferromagnetically ordered, the hybridization between the Fe3d and Mo4d states pushes up (down) the Mo4$d_\uparrow$ (Mo4$d_\downarrow$) states located between the Fe3$d_\uparrow$ and Fe3$d_\downarrow$ levels. Then, the electrons near E_F transfer from the Mo4$d_\uparrow$ state to the Mo4$d_\downarrow$ state. Resultant kinetic energy gain stabilizes the ferromagnetic state, as compared with the antiferromagnetic (or the paramagnetic) states.

In the latter two pictures, the magnetic moment at the Mo site is merely induced by the Fe magnetic moment through the hybridization between the Fe3d and Mo4d states. In this sense, the present system is *not ferrimagnetic but ferromagnetic*. Our experimental results are consistent with these pictures.

IV. SUMMARY

We have investigated the electron doping effects on the magnetic and electronic properties in the conducting double-perovskite molybdenum oxides $(Sr_{2-x}La_x)FeMoO_6$. The LDA+U band calculation indicates that the down-spin conduction band near E_F has a considerable amount of the Fe3$d_\downarrow(t_{2g\downarrow})$ component, reflecting the strong hybridization between the Fe3d and Mo4d states. This is consistent with the x dependence of the magnetic and electronic properties as well as the suppressed μ_{Fe} and μ_{Mo} To clarify the significant role of the Mo4d-Fe3d hybridization on the magnetism, spectroscopic investigations are indispensable.

ACKNOWLEDGMENTS

The authors are grateful to J. Kanamori for fruitful discussion on the origin for the magnetism of this system. This work was supported by a Grant-In-Aid for Scientific Research from the Ministry of Education, Science, Sports and Culture. The synchrotron power experiments were performed at the SPring-8 BL02B2 with approval of the Japan Synchrotron Radiation Research Institute (JASRI).

[1] P.W. Anderson and H. Hasegawa, Phys. Rev. **100**, 675 (1955).
[2] M.T. Anderson, K.B. Greenwood, G.A. Taylor, and K.R Poeppelmeier, Prog. Solid State Chem. **22**, 197 (1993).
[3] F. Galasso, F.C. Douglas, and R. Kasper, J. Chem. Phys. **44**, 1672 (1966).
[4] F.K. Patterson, C.W. Moeller, and R. Wald, Inorg. Chem. **2**, 196 (1963).
[5] J. Longo and R. Wald, J. Am. Chem. Soc. **83**, 2816 (1961).
[6] Y. Moritomo, Sh. Xu, A. Machida, T. Akimoto, E. Nishibori, M. Takata, and M. Sakata, Phys. Rev. B **61**, R7827 (2000).
[7] K.-I. Kobayashi, T. Kimura, H. Sawada, K. Terakura, and Y. Tokura, Nature (London) **395**, 677 (1998); K.-I. Kobayashi, T. Kimura, Y. Tomioka, H. Sawada, K. Terakura, and Y. Tokura, Phys. Rev. B **59**, 11 159 (1999).
[8] T.H. Kim, M. Uehara, S.-W. Cheong, and S. Lee, Appl. Phys. Lett. **74**, 1737 (1999).
[9] H.-Y. Hwang, S-W. Cheong, P.G. Radaelli, M. Marezio, and B. Batlogg, Phys. Rev. Lett. **75**, 914 (1995).
[10] Y. Tomioka, T. Okuda, Y. Okimoto, R. Kumai, K.-I. Kobayashi, and Y. Tokura, Phys. Rev. B **61**, 422 (2000).
[11] Y. Moritomo, S. Xu, A. Machida, T. Akimoto, E. Nishibori, M. Takata, M. Sakata, and K. Ohoyama, J. Phys. Soc. Jpn. **69**, 1723 (2000).
[12] Y. Moritomo, H. Kusuya, T. Akimoto, and A. Machida, Jpn. J. Appl. Phys., Part 2 **39**, L360 (2000).
[13] M. Takata, E. Nishibori, K. Kato, M. Sakata, and Y. Moritomo, J. Phys. Soc. Jpn. **68**, 2190 (1999).
[14] F. Izumi *The Rietveld Method*, edited by R.A. Young (Oxford University Press, Oxford, 1993), Chap. 13; Y.-I. Kim and F. Izumi, J. Ceram. Soc. Jpn. **102**, 401 (1994).
[15] I. Mannari, Prog. Theor. Phys. **22**, 335 (1959).
[16] Y. Moritomo, A. Asamitsu, and Y. Tokura, Phys. Rev. B **51**, 16 491 (1995).
[17] K. Ohoyama, T. Kanouchi, K. Nemoto, M. Ohashi, T. Kajitani, and Y. Yamaguchi, Jpn. J. Appl. Phys., Part 1 **37**, 3319 (1998).
[18] Determination of the spin direction is difficult, due to the quasicubic structure.
[19] O.K. Andersen, Phys. Rev. B **12**, 3060 (1975); T. Takeda and J. Kubler, J. Phys. F **9**, 661 (1979).
[20] P. Hohenberg and W. Kohn, Phys. Rev. **136**, B864 (1964); W. Kohn and L.J. Sham, *ibid.* **140**, A1133 (1965); S.H. Vosko, L. Wilk, and M. Nusair, Can. J. Phys. **58**, 1200 (1980).
[21] V.I. Anisimov, J. Zaanen, and O.K. Andersen, Phys. Rev. B **44**, 943 (1991); V.I. Anisimov, F. Aryasetiawan, and A.I. Lichtenstein, J. Phys.: Condens. Matter **9**, 767 (1997); I. Solovyev, N. Hamada, and K. Terakura, Phys. Rev. B **53**, 7158 (1996).
[22] J. Kanamori and K. Terakura (unpublished).